

INFERRING THE LINEAR POWER SPECTRUM FROM THE LYMAN- α FOREST

MATIAS ZALDARRIAGA¹, ROMÁN SCOCCIMARRO¹, & LAM HUI²

¹Physics Department, New York University, 4 Washington Place, New York, NY 10003

²Department of Physics, Columbia University, 538 West 120th Street, New York, NY 10027

October 24, 2018. To be submitted to ApJ.

ABSTRACT

We discuss the determination of the linear power spectrum of dark matter fluctuations from measurements of the transmitted flux Ly- α Forest power spectrum. We show that on most scales probed by current measurements, the flux power spectrum is significantly affected by non-linear corrections to the linear dark matter power spectrum due to gravitational clustering. Inferring the linear dark matter power spectrum shape is therefore difficult due to non-linear corrections driving the non-linear power spectrum to a $k^{-1.4}$ shape nearly independent of initial conditions. We argue that some methods used in previous estimates underestimate the uncertainties in the shape of the linear dark matter power spectrum.

Subject headings: cosmology: theory – intergalactic medium – large scale structure of universe; quasars – absorption lines

1. INTRODUCTION

In the last few years the Lyman α forest has become increasingly important as a probe for cosmology. The availability of high resolution high signal-to-noise spectra, mainly from the HIRES spectrograph on the Keck telescope, has revolutionized the field. The data have been compared with the theoretical predictions of currently favored cosmological models, mainly using numerical simulations (Cen et al. 1994, Hernquist et al. 1995, Zhang et al. 1995, Miralda-Escude et al. 1996, Muecket et al. 1996, Wadsley & Bond 1996, Theuns et al. 1998). The success of these models has been impressive. The observed properties of the forest are very well reproduced even though the models were primarily constructed in the context of galaxy clustering – this was a non-trivial accomplishment. Examples of comparisons of model predictions with observational data can be found in Croft et al. (1998), Bryan et al. (1999), McDonald et al. (1999, 2000), Nusser & Haehnelt (2000), Schaye et al. (1999, 2000), Croft et al. 2000, Meiksin, Bryan & Machacek (2001), Choudhury, Srianand & Padmanabhan (2001), Zaldarriaga, Hui & Tegmark (2000) (ZHT2000), and Pichon et al. (2001). The same cosmological models also produce acceptable fits to many other cosmological observations such as the power spectra of CMB fluctuations, the luminosity distance to high redshift supernovae, the number density of massive clusters, etc. (see Wang, Tegmark & Zaldarriaga 2000 for a recent summary).

The success of the numerical models of the forest has also led to the construction of several analytic approximations (e.g. Bi & Davidsen 1997, Gnedin & Hui 1996, Hui et al. 1997b, Viel et al. 2001, Schaye 2001). The physics that is responsible for the absorption seems to be well understood so the hope has emerged that we could use the Lyman- α forest to further constrain cosmological models. The advantages of the forest over other observations are clear, since we get to observe the universe at an earlier time we may be able to infer the rate of growth of density fluctuations. It is also assumed that because we are observing at a higher redshift, scales that today (e.g. in galaxy surveys)

are in the “non-linear regime”, can be probed when they are still “linear”, thus greatly simplifying the analysis. In this paper, we challenge this assumption.

Studies of the forest have other applications. Through the Alcock-Paczynski test (Alcock & Paczynski 1979) applied to the correlation functions for pairs of lines of sight, it seems possible to directly infer the geometry of the universe (Hui, Stebbins & Burles 2000, McDonald & Miralda-Escude 2000, McDonald 2001). Higher order statistics of the flux may also prove useful in testing that the structure observed in the flux is actually produced by gravitational instability (Zaldarriaga, Seljak & Hui 2001) and in testing if there are fluctuations in the temperature of the IGM, left for example as remnants of a late ionization of Helium II (Zaldarriaga 2001, Theuns et al. 2001).

The power spectrum of the flux is perhaps the most studied of the statistics of the Lyman α forest flux. Inferring cosmological parameters from the power spectrum is however a difficult challenge. A naive approach would be to run hydrodynamical simulation for enough models to cover the parameter space of interest and compare the results with the observed data. This approach is impractical as the computer time needed to run the number of simulations required is enormous. One should also remember that on top of the usual cosmological parameters that are needed to specify the cosmological model (*i.e.* the energy densities in the different components and the power spectrum of initial density fluctuations) in the case of the forest one needs to specify the time evolution of the background of ionizing radiation that is responsible for ionizing and heating the gas. This requires the introduction of additional parameters. One should also keep in mind that even if we were able to run a large enough grid of hydrodynamical simulations, it is not obvious that all the relevant physics is correctly included in these simulations, “feedback” effects from the forming stars and galaxies being the obvious example (see e.g. Meiksin, Bryan & Machacek 2001 for possible conflicts with observations).

A significant simplification can be achieved with the introduction of the N-body model of the forest. In this model the spatial distribution of the dark matter is ob-

tained by running an N-body simulation. The gas is then assumed to trace the dark matter (or maybe a smoothed version of the dark matter field to account for the effect of gas pressure). Furthermore it is assumed that the gas is in photo-ionization equilibrium and follows a power-law equation of state. This simple prescriptions lead to a simulated Lyman α forest that is in reasonable agreement with the predictions of full hydro simulations. As could have been expected, the agreement is good but not perfect (Meiksin & White 2000). The great advantage of the N-body approximation is that it significantly reduces the computational burden of exploring parameter space. A first attempt at implementing the straightforward method of running a grid of N-body simulations and comparing that with the forest data to extract parameters was presented in ZHT2000.

In the quest of incorporating data from the forest to studies of cosmological parameters even the N-body model is computationally too expensive. This has lead to the introduction of approximate techniques to invert the observed flux power spectrum to get the 3D *linear* matter power spectrum of the dark matter. The results of these inversions are then compared to any model of interest and the results of these comparisons are used to constrain parameters. It is clear that the inversion method greatly simplifies the comparison between theory and observations, which only requires the ability to predict the *linear* power spectrum of any given model, a straightforward task. Obviously the relation between the linear dark matter power spectrum and the flux power spectrum is non-trivial, so these inversions are not rigorous inversions in the mathematical sense. The resulting prescriptions, however, are calibrated with numerical simulations, and are the result of detailed studies of the physics of the forest (Croft et al. 2000).

The aim of this paper is to point out the limitations of inversion techniques which attempt to match predictions of the forest from knowledge of the linear power spectrum of dark matter. In particular, we point out that the evolution of fluctuations at $z \sim 3$ is significantly non-linear at scales that can be orders of magnitude larger than estimated by naive linear arguments. Furthermore, non-linear corrections tend to drive the density (and velocity) field to “universal” spectra nearly independent of initial conditions, erasing information and leading to weak constraints on the shape of the primordial dark matter power spectrum.

The rest of this paper is organized as follows. In §2 we summarize the constraints on the primordial power spectrum that we obtain by running a grid of N-body simulations and compare them with those obtained by the inversion technique described above. The remaining sections present what we believe to be the main reasons behind these results. In §3 we discuss the role of non-linear corrections, in §4 we discuss the effects of the transformation between density and flux and the importance of redshift distortions. We conclude in §5.

2. LIKELIHOOD FROM N-BODY SIMULATIONS

Our first objective is to convince the reader that there are problems with the error bars that result from inversion methods. We use the technique described in ZHT2000 to find constraints on the amplitude and slope of the linear

power spectrum of dark matter fluctuations. Basically we run a grid of P^3M N-body simulations of the standard CDM model in boxes of size $L = 16 h^{-1} \text{Mpc}$. We choose a range of spectral indices for the primordial power spectrum, ($n_p = 0.4, 0.7, 0.9, 1.0, 1.1, 1.3, 1.7$), $n_p = 1$ corresponding to the usual scale-invariant spectrum, and store the outputs at several different times, corresponding to scale factors $a = (.05, .065, .085, .11, .14, .19, .24, .31, .41)$.

The relation between gas density and dark matter density is modeled by introducing additional parameters. To model the effects of pressure we smooth the density field with a three-dimensional smoothing scale we call k_f . For simplicity we used a Gaussian window, $W(k) = \exp(-(k/k_f)^2)$ as described in ZHT2000. The smoothing scale k_f is related to the Jeans scale k_J by,

$$k_f = \eta k_J; \quad k_J = ac_s^{-1} \sqrt{4\pi G \bar{\rho}}, \quad (1)$$

where c_s is the sound speed of the gas and η is a function of time and the details of the ionization history with values around $\eta \sim 2$ for standard assumptions (Gnedin & Hui 1998). Equation (1) leads to,

$$k_f \approx 30 h \text{Mpc}^{-1} \times \left(\frac{\eta}{2}\right) \left(\frac{h}{0.7}\right)^{-1} \times \left(\frac{\Omega_m h^2}{0.15}\right)^{1/2} \left(\frac{1+z}{4}\right)^{1/2} \left(\frac{T}{10^4 \text{K}}\right)^{1/2} \left(\frac{kT}{c_s^2 m_p}\right)^{1/2}, \quad (2)$$

where m_p is the mass of the proton.

The equation of state of the gas is described by two parameters, the temperature at zero overdensity T_0 and the slope α , $T = T_0(1 + \delta)^\alpha$ where δ is the overdensity (Hui & Gnedin 1997a). The optical depth of a given fluid element is given by $\tau = A(1 + \delta)^\beta$, the assumption of ionization equilibrium leads to $\beta = 2 - 0.7\alpha$. The amplitude A , which physically depends on the strength of the ionizing background, is chosen so that the constructed spectra have the observed mean transmission which we call \bar{F} . For each simulation we construct grids of model predictions with $(k_f, T_0, \alpha, \bar{F})$ as parameters. Our full parameter vector $\mathbf{p} = (a, n_p, k_f, T_0, \alpha, \bar{F})$ has 6 dimensions.

For each model in our six dimensional space we calculate the predicted flux power spectrum $P_f(\mathbf{p})$. We compare these prediction to the data and compute a likelihood function as described in ZHT2000. We used a Gaussian approximation for the likelihood,

$$\mathcal{L}(\mathbf{d}; \mathbf{p}) \propto \prod_i \exp \left[-\frac{1}{2} \left(\frac{d_i - P_{fi}(\mathbf{p})}{\sigma_i} \right)^2 \right], \quad (3)$$

where i runs over the different data points d_i , the model prediction for that wavevector are $P_{fi}(\mathbf{p})$ and σ_i are the error bars on each point. To obtain one dimensional constraints on individual parameters or two dimensional constraints for a pair of parameters, we marginalized the likelihood one parameter at a time, reducing the dimensions of the grid by one in each step until only the parameter or pair of parameters of interest was left.

When marginalizing over parameters we allow \bar{F} to vary within observational constraints. At $z = 2.72$ corresponding to the mean redshift of the sample used we take $\bar{F} = 0.707 \pm 0.035$, a 5% uncertainty. We should

note that we have added in quadrature a “theoretical uncertainty” to the observational errors. This extra uncertainty was estimated from the fluctuations in the mean flux computed in different realizations of the same model and could be improved upon with better simulations. We include the constraints on \bar{F} by multiplying the likelihood coming from the forest power spectrum by $\exp(-\delta\chi^2/2)$, with $\delta\chi^2 = [(\bar{F} - 0.707)/0.035]^2$.

In ZHT2000 we presented constraints on the primordial power spectrum. In that paper we were mainly interested in the effects of the temperature and the constraints that could be obtained on it. The temperature smooths the spectra and we wanted to make sure that we did not underestimate the uncertainties by assuming we knew what k_f , the other source of smoothing, actually was. For that reason we had a grid in k_f that was too conservative, $k_f = (5, 10, 20, 30, 40, 45, 50, 55, 60, 70, 80)h \text{ Mpc}^{-1}$. The smallest values in this grid (the largest smoothings) produce much more smoothing than can be expected from pressure. However because k_f smooths the field in 3D before we apply the non-linear transformation that takes density to optical depth and flux, while T_0 acts in 1D smoothing the optical depth, we were able to distinguish between them. We also found that the k_f smoothing was quite degenerate with the spectral index of the perturbations n so our constraints on that parameters were weak.

In this paper we improve on the earlier analysis by using newer data from Croft et al. (2000). We use the power spectra of their “fiducial sample” which has mean redshift $z = 2.72$ (table 3 of Croft et al. 2000). The sample was compiled using data from the Low Resolution Imaging Spectrometer (LRIS) and the High Resolution Spectrometer (HIRES) on the Keck Telescope. Data in the redshift range $2.3 < z < 2.9$ with a total path length $\delta z \approx 25$ was used to create the “fiducial sample” (Croft et al. 2000). As another improvement in our marginalizations we restrict the k_f grid to values $k_f > 30h \text{ Mpc}^{-1}$. With the improved data and a more physical “prior” for k_f we hope to find tighter constraints on the primordial power spectrum.

In figure 1 we show our constraints in the $\Delta_*^2 - n_{\text{eff}}$, the amplitude and slope of the linear power at a scale $k_p = 0.03 \text{ (km/s)}^{-1}$. That is $\Delta^2(k) = 4\pi k^3 P(k)$ and $\Delta^2(k_p) = \Delta_*^2$ with $(d \ln \Delta^2(k)/d \ln k)|_{k_p} = n_{\text{eff}} + 3$. To illustrate the effect of the uncertainty in k_f we show the results if we marginalize over k_f with the restriction $k_f > 30h \text{ Mpc}^{-1}$ or if we just assume $k_f = 30h \text{ Mpc}^{-1}$. For comparison we also plot the results obtained by Croft et al. 2000 with the inversion technique. Note that when we marginalize over k_f , that is when we allow smaller k_f smoothing scales, models with smaller spectral indices become allowed. This makes sense because one can compensate for the lack of power in the dark matter by assuming that the smoothing due to pressure is smaller.

Figure 1 shows that we find acceptable models outside the range inferred from the inversion technique. In figure 2 we show examples of such models. The two models have very different spectral indices of the linear power spectrum, one has $n_p = 0.7$ ($n_{\text{eff}} = -2.7, \Delta_*^2 = 0.42$) and the other has $n_p = 1.3$ ($n_{\text{eff}} = -2.3, \Delta_*^2 = 0.57$). Part of the increase in the allowed range of Δ_*^2 seen in figure 1 comes from our more conservative choice of errors for \bar{F} . Unfortunately, the relation between the amplitudes of the dark

matter and flux power spectrum is very sensitive to \bar{F} , a quantity that is sensitive to small scale physics and may not be very well modeled by dark matter only simulations. Figures 1 and 2 clearly show that the inversion technique underestimates the errors, thus results from such studies should be interpreted with care if one wants to incorporate them to likelihood analysis of cosmological parameters.

It is important to understand that the non-linear corrections make the power spectra of the two models under consideration look similar but that in order to fit the data we must allow some extra freedom in another parameter to accommodate the residual differences. In the example shown, α had to vary between 0.1 and 0.3. This means that if there are independent ways (not using the power spectrum) to measure α , and in general the equation of state, then the error-bar on n can conceivably be reduced. Using the b-parameter-column density distribution might be one way of achieving this, but the error on α is at present still quite large (eg. Ricotti et al. 2000, Schaye et al. 2000, McDonald et al. 1999, Bryan et al. 1999, Hui & Rutledge 1999).

We should emphasize that the error-bars we find using our grid method are likely to underestimate the real uncertainties because we do not include uncertainties associated with hydrodynamic effects. Nonetheless, it is possible that our uncertainties are larger than they should be. For example, the smoothing due to pressure (k_f), the temperature of the gas and the slope of the equation of state can all be determined once the ionization history is known [i.e. equations (1) and (2) for k_f]. However we are allowing them to vary independently in our marginalization. This means that if we were to factor in some “physical priors” that restricted these parameters or forced relations between them, our constraints could get tighter.

The aim of the following sections is to try to identify what is causing the increased uncertainties.

3. NON-LINEAR CORRECTIONS: CRITICAL INDEX

The scales probed by the Lyman- α forest at $z \sim 3$ correspond to values of the linear mass power spectrum $P_L(k)$ where $4\pi k^3 P_L(k) \sim 0.01 - 1$. This may suggest that these scales are safely in the linear regime. However, the amplitude of linear fluctuations is not the only quantity that determines the magnitude of non-linear corrections. The other important quantity is the spectral index at scales in the weakly non-linear regime (Makino, Sasaki & Suto 1992; Lokas et al. 1996; Scoccimarro & Frieman 1996). For typical CDM models, the effective spectral index n_{eff} at the non-linear scale (k_{nl} such that $4\pi k_{\text{nl}}^3 P_L(k_{\text{nl}}) \equiv 1$) is quite negative $n_{\text{eff}} \lesssim -2.5$ (e.g. compared to $z = 0$ where $n_{\text{eff}} \sim -1.5$). This means that non-linear corrections are large, since for steep spectra gravitational collapse is driven by large-scale coherent flows which substantially enhance the growth of density perturbations compared to the linear case. In fact, for power-law initial spectra we can write the non-linear mass power spectrum in one-loop perturbation theory (PT) as (Scoccimarro & Frieman 1996)

$$P(k) = P_L(k) \left[1 + \alpha(n) \left(\frac{k}{k_{\text{nl}}} \right)^{n+3} \right], \quad (4)$$

where $\alpha(n)$ is a function of spectral index which mono-

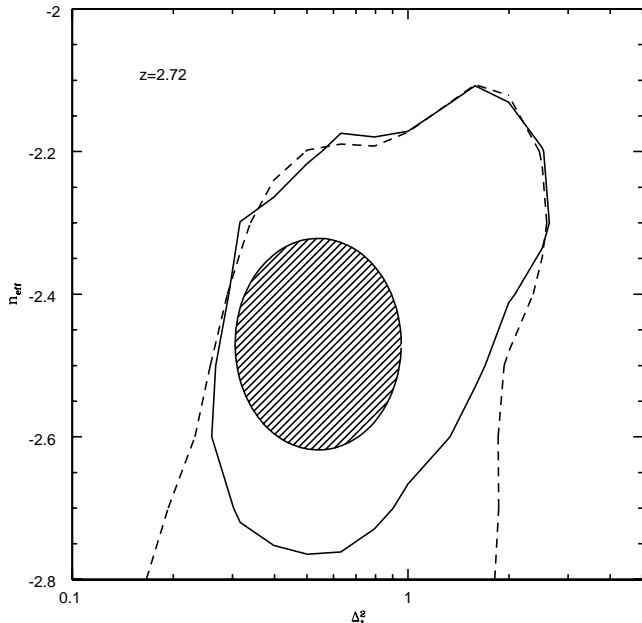


FIG. 1.— Constraints in the $\Delta - n_{\text{eff}}$ plane. The solid line shows constraints when we fix $k_f = 30h \text{ Mpc}^{-1}$, the dashed curve is when we allow $k_f > 30h \text{ Mpc}^{-1}$. In both cases the lines correspond to an increase of $\delta\chi^2 = 6.17$ with respect to the best model (95% confidence for a Gaussian). The dashed circle are constraints obtained using the inversion technique and the same data by Croft et al. 2000.

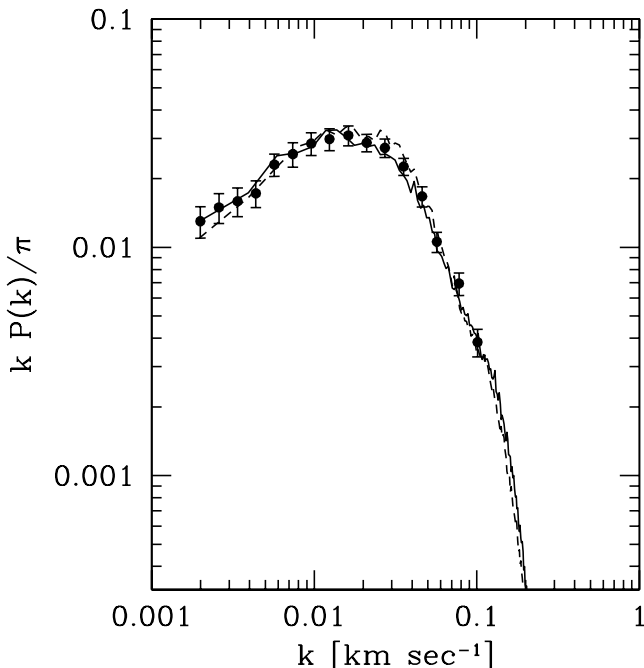


FIG. 2.— Transmission power spectrum from Croft et al. (2001) together with two models that are acceptable fits. The two models have parameter vectors $\mathbf{p} = (0.19, 0.7, 30, 250, 0.1, 0.684)$ and $\mathbf{p} = (0.11, 1.1, 30, 250, 0.3, 0.684)$.

tonically decreases with n , becoming larger than unity for $n < -1.7$. For $n < -1.4$, the non-linear correction is positive, leading to a non-linear spectrum less steep than the linear one. For $n \approx -1.4$, α becomes zero and thus the

power spectrum retains its linear shape. For $n > -1.4$, the non-linear corrections are actually negative, so the non-linear power spectrum grows slower than in linear PT, becoming steeper than the linear spectrum. As a result of this, the non-linear power spectrum is driven towards a “critical index” $n_c = -1.4$, regardless of its linear slope (Scoccimarro & Frieman 1996). Although Eq. (4) is valid rigorously only for a power-law spectrum, CDM spectra behave in the same way, as seen in Fig. 3. Note how the shape of the non-linear power spectrum becomes $\sim k^{-1.4}$ (dashed line) even at $k < k_{\text{nl}}$. In fact all the scales shown in the figure are below k_{nl} for the model with $n_p = 0.7$. Similar behavior is seen in Fig. 1 of Narayanan et al. (2000) and Fig. 3 of White & Croft (2000) for CDM models with truncated linear spectra.

Figure 4 illustrates the importance of non-linear corrections as a function of power spectrum normalization σ_8 , for linear power spectra with shape parameter $\Gamma = 0.21$ (dashed), $\Gamma = 0.15$ (dot-dashed) and $\Gamma = 0.1$ (solid), which approximately span the range of spectral indices obtained in figure 1. The calculation was done using one-loop perturbation theory¹. The scales where linear (top three lines) and non-linear (middle lines) fluctuations are of order unity and where non-linear corrections are 20% (bottom lines) all agree at large σ_8 , where the spectral index at the non-linear scale is about $n_{\text{eff}} \sim -1.5$. At low σ_8 , the effective spectral index at weakly non-linear scales becomes much more negative, leading to stronger non-linear corrections. The wavenumber at which non-linear corrections are 20% can thus be a very small fraction of the non-linear scale (estimated either from the linear or the non-linear power spectrum). For the normalizations corresponding to $z \sim 3$ (denoted by the horizontal bar in figure 4), the wavenumber at which non-linear corrections become important can be orders of magnitude smaller than that estimated from linear perturbation theory. In particular, note that models with more negative spectral index (lower Γ) require higher σ_8 to match the fluctuation amplitude at the scales probed by the Ly- α forest, thus these models are most strongly affected by non-linear effects, at wavenumbers as small as $k \sim 0.004 \text{ km/sec}$.

The outcome of this situation is that at $z \sim 3$ non-linear corrections are important at scales of interest for the Ly- α forest and drive the mass power spectrum to a $k^{-1.4}$ dependence. Therefore, measuring the Ly- α flux power spectrum at these scales does not give a direct probe of the initial, linear, shape of the dark matter power spectrum, leading to degeneracies in the range of initial shapes constrained by the data, as shown in figure 1. This is illustrated rather clearly by comparing figures 2 and 3, where significantly different linear spectra display very similar transmission power spectra. However, before we can establish that non-linear dynamics is the main reason behind the observed behavior, we must consider other non-linear effects that potentially enter: the non-linear mapping between the dark matter density field and Ly- α transmission, and the effects of redshift distortions.

4. FLUX CORRELATIONS: A SIMPLE MODEL

The discussion in the previous section was in terms of the dark matter density field δ . However, as we show be-

¹If anything, this calculation underestimates non-linear effects.

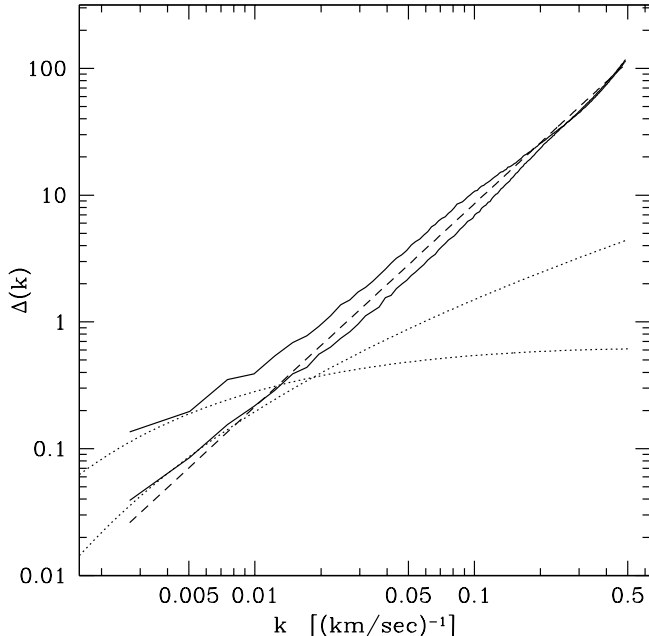


FIG. 3.— Linear (dotted) and non-linear (solid) dark matter power spectra for two models with primordial spectral index $n_p = 0.7$ (top) and $n_p = 1.3$ bottom, corresponding to the transmission power spectra shown in figure 2. Note how non-linear corrections are very large for the $n_p = 0.7$ case, even though the linear spectrum suggests linear PT should be accurate. Non-linear dynamics tends to establish a power spectrum with a critical index $n = -1.4$, as shown by the dashed line.

low, there is a relevant range of scales for which the picture described above applies as well to the transmitted Ly- α flux power spectrum. The reason is that the characteristic wavenumber for which the non-linear nature of the mapping between δ and F enters, the smoothing scale wavenumber² $k_{SM} \sim 0.05$ (km/sec)⁻¹, is much larger than the wavenumber where non-linear corrections in the density field become important (see figures 3-4).

We take a simple toy model to illustrate our arguments. The transmitted flux $F = \exp(-\tau)$ is approximated as $F = \exp[-A(1+\delta)^2]$ and δ is the density field assumed to be Gaussian for the moment (we will relax this assumption below). In this case, the mean transmission is given by

$$\bar{F} = \frac{1}{\sqrt{1+2A\sigma^2}} \exp\left[\frac{-2A}{1+2A\sigma^2}\right] \quad (5)$$

We work in terms of the flux contrast, $\delta_F \equiv F/\bar{F} - 1$, then the two-point function of δ_F reads,

$$1 + \langle \delta_F(1)\delta_F(2) \rangle \equiv 1 + \xi_F \\ = \frac{(1+2A\sigma^2)}{\sqrt{1+4A\sigma^2+4A^2(\sigma^4-\xi^2)}} \quad (6)$$

²The sharp, exponential decline in the flux power spectrum seen in figure 2 is due to thermal broadening. The scale k_{SM} is related to the thermal broadening scale $k_{TH} \approx 0.1$ (km/sec)⁻¹ by the non-linear mapping from optical depth to transmission power spectrum; this follows from Eq. (7) below. That is, for a given value of \bar{F} and σ^2 , ξ_F/σ_F is a function of ξ/σ . Then, smoothing in the optical depth (approximately density) can be translated into smoothing in the transmission power spectrum. For $\sigma \gtrsim 1$, $k_{SM} < k_{TH}$.

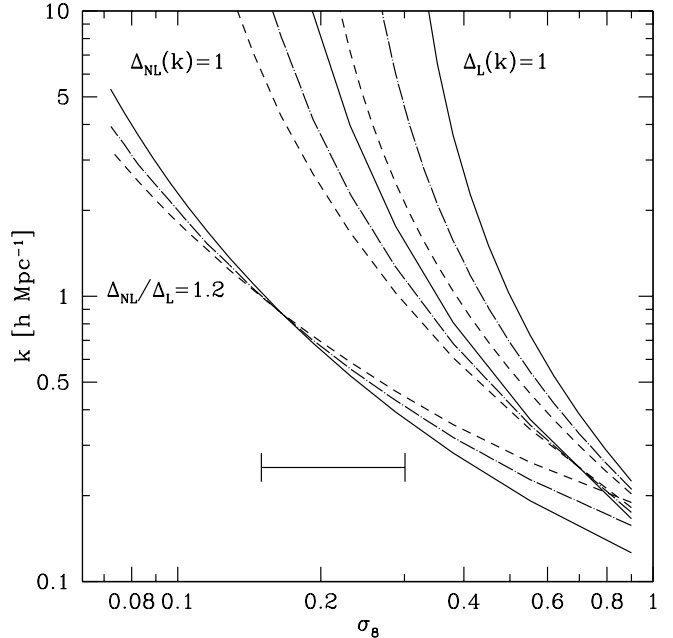


FIG. 4.— The importance of non-linear effects, as a function of σ_8 for linear power spectra with shape parameter $\Gamma = 0.21$ (dashed), $\Gamma = 0.15$ (dot-dashed) and $\Gamma = 0.1$ (solid). The three lines denote the non-linear scale according to linear spectrum (top), non-linear spectrum (middle), and the scale at which non-linear corrections are 20%. At low redshift, high σ_8 , all these scales coincide, approximately. At high redshift, small σ_8 , non-linear corrections are much larger and thus become important at wavenumbers that can be a very small fraction of the non-linear scale. The horizontal bar denotes approximately the range of normalizations for $z \sim 3$. Note that translation from h/Mpc to inverse velocity units is given by $k_v = k/(aH) \approx k/H_0[\Omega_m^0(1+z)]^{-1/2}$ at high z , where $\Omega_m^0 = \Omega_m(z=0)$. For Λ CDM with $\Omega_m^0 = 0.3$, $\Omega_\Lambda^0 = 0.7$, $k_v = k/111.5$ at $z = 3$.

$$\times \exp\left[\frac{4A^2\xi}{(1+2A\sigma^2)[1+2A(\sigma^2+\xi)]}\right],$$

where ξ is the two-point function of the density field. Note that in the limit where $\xi \ll \sigma^2$ (but *not* necessarily $\xi < 1$, since $A\sigma^2$ cannot be large due to the mean flux in Eq. (5) being of order unity), the above expression reduces to,

$$\xi_F = \frac{4A^2}{(1+2A\sigma^2)^2} \xi \equiv b^2\xi \quad (7)$$

Thus, in this case the flux correlation function is proportional to the density correlation function with some bias factor. This is certainly expected at large scales, since the flux is a local transformation of the density contrast, it follows from well-known arguments (e.g. Fry & Gaztañaga 1993, Scherrer & Weinberg 1998) that the correlation function of the flux should be proportional to that of the underlying density field. The bias factor in this simple model, Eq. (7), can be shown to change by a factor of about two when the the mean flux, Eq. (5), changes within its 2σ interval, similar to the variations seen in Fig. 17 of Croft et al. (2000). Equivalently figure 10c of McDonald (2001) shows that a 3% change in the mean flux can lead to a 40% change in the power spectrum amplitude.

As pointed out above, the validity of Eq. (7) is not restricted to the linear regime, since there are other small

parameters that enter. The value of $A\sigma^2$ is controlled by the mean flux as given by Eq. (5). Since the mean flux has to be between 0 and 1, in particular $\bar{F} \approx 0.7$, $A\sigma^2$ is constrained to be smaller than unity³, even in the limit that $\sigma^2 \gg 1$. Eq. (7) then follows as long as $\xi \ll \sigma^2$, irrespective of the value of ξ (since $A\sigma^2 \lesssim 1$, $A\xi \ll 1$ in this regime). The condition that $\xi \ll \sigma^2$ means in the Ly- α case that the scales under consideration be much larger than the thermal broadening scale, $k \ll k_{\text{TH}}$, the characteristic smoothing scale where σ^2 is evaluated. This is in any case where most of the information can be extracted, so the approximations leading to Eq. (7) are physically relevant.

Of course, when ξ approaches unity, the Gaussian model for the density field PDF is not a good approximation anymore. In order to see how the arguments above generalize to the non-Gaussian case, let's consider the expansion of the two-point PDF when $\xi \ll \sigma^2$,

$$P(\delta_1, \delta_2) \approx P(\delta_1)P(\delta_2) [1 + b(\delta_1)b(\delta_2) \xi], \quad (8)$$

where $b(\delta) = \delta/\sigma^2$ in the Gaussian case. Although the relation in Eq. (8) was written starting from a Gaussian PDF, its validity is much more general. It can be obtained rigorously in the weakly non-linear regime (in tree-level PT, Bernardeau 1996), and in the highly non-linear regime for factorizable hierarchical models (Bernardeau & Schaeffer 1999), where specific predictions for the function $b(\delta)$ can be given in both cases. Then, the linear relation in Eq. (7) between ξ_F and ξ continues to hold, but with a different bias factor than in the Gaussian case. Note that in the hierarchical model, ξ is understood to be the fully non-linear correlation function.

These two examples, however, are not exactly relevant for structure formation at $z \sim 3$ at the scales of interest. Tree-level PT is not a good approximation because the spectral index at the non-linear scale is so negative $n_{\text{eff}} \lesssim -2.5$ that loop corrections to moments of the density field are very important, as noted above for the power spectrum. On the other hand, we cannot assume a factorizable hierarchical model, which is expected to become a good approximation only in the highly non-linear regime.

However, the structure of loop corrections still respects Eq. (8) in the following broad sense. Consider the calculation of connected two-point moments, $\langle \delta_1^p \delta_2^q \rangle_c$, which fully characterize the connected two-point PDF. At large scales it follows that (Bernardeau 1996)

$$\langle \delta_1^p \delta_2^q \rangle_c = C_{pq} \sigma_L^{2(p+q-2)} \xi_L, \quad (9)$$

where C_{pq} are numbers that depend weakly on scale through derivatives of the linear variance and smoothed two-point function with respect to scale (L denotes linear quantities). Since all connected moments are proportional to ξ_L , the connected two-point PDF should also be proportional to ξ_L , as in Eq. (8), where ξ is replaced by ξ_L . In addition, it can be shown that $C_{pq} = C_{p1}C_{q1}$, which leads directly to the factorization $b(\delta_1)b(\delta_2)$, with $b(\delta)$ calculable from tree-level PT. As loop corrections are included, a subset of loop diagrams will lead to non-linear corrections

³This can break down for non-Gaussian distributions, since as σ increases the PDF becomes more peaked about $\delta = -1$ and one can thus tolerate a larger A . For the models discussed in Section 2, $A\sigma^2 \approx 1$.

to ξ_L and σ_L^2 in Eq. (9), making $\xi_L \rightarrow \xi$ and $\sigma_L^2 \rightarrow \sigma^2$ in Eq. (9). In addition, there will be new links in the diagrams leading to higher powers of ξ_L and σ_L^2 ; however, at a given order in PT since $\xi_L \ll \sigma_L^2$ the latter are much more important than the former. As a result of this, we expect that as non-linear scales are probed, as long as $\xi \ll \sigma^2$, Eq. (9) becomes

$$\langle \delta_1^p \delta_2^q \rangle_c \sim C_{pq}(\sigma) \sigma^{2(p+q-2)} \xi, \quad (10)$$

where we have absorbed additional σ dependence into C_{pq} . Note that this also respects the scaling expected in the highly non-linear regime, as long as $C_{pq}(\sigma) \rightarrow \text{const.}$ as $\sigma \rightarrow \infty$. Recent studies of the behavior of $\langle \delta_1^p \delta_2^q \rangle_c$ as a function of σ and ξ in numerical simulation support the above arguments for $\xi \ll \sigma^2$ (Gaztañaga, Fosalba & Croft 2001). However, one must keep in mind that they studied CDM models at $z = 0$ rather than $z \sim 3$ as concerns us here⁴.

Now let's consider the effect of redshift distortions. In this case, the redshift-space position $\mathbf{s} = \hat{\mathbf{x}} - f u_z(\hat{\mathbf{x}})$, where $f \approx \Omega_m^{0.6} \approx 1$ at the redshifts of interest and u_z is the line of sight velocity, normalized by the Hubble constant so that in linear PT, $\nabla \cdot \mathbf{u} = \delta$. The transformation between optical depth in real and redshift space reads $\tau_s ds = \tau dz$ (e.g. Hui et al. 1997b; Gaztañaga & Croft 1999) with $ds = J dz$ and $J = |1 - f \nabla_z u_z|$. This leads to a *three-dimensional* flux power spectrum (following the calculation in Scoccimarro, Couchman & Frieman 1999),

$$P_s^F(\mathbf{k}) = \int d^3r e^{i\mathbf{k} \cdot \mathbf{r}} \langle e^{ik_z f \Delta u_z} J_1 J_2 e^{-\tau_1/J_1} e^{-\tau_2/J_2} \rangle, \quad (11)$$

where $\mathbf{r} \equiv \hat{\mathbf{x}}_1 - \hat{\mathbf{x}}_2$ and $\Delta u_z \equiv u_z(\hat{\mathbf{x}}_1) - u_z(\hat{\mathbf{x}}_2)$. At large scales, one is allowed to expand all the exponential factors and use $\delta, \nabla_z u_z \ll 1$, in which case $e^{ik_z f \Delta u_z} J_1 J_2 \approx 1 + \mathcal{O}(\nabla_z u_z)^2$, and the remaining exponentials give $P_s^F(k) = (A\nu)^2 (1 + \beta\mu^2)^2 P_L(k)$ (Hui 1999), where we assumed $\tau \equiv A(1 + \delta)^\nu$ and $\mu \equiv k_z/k$, $\beta \equiv f/\nu$. This is analogous to the standard result for the galaxy redshift-space power spectrum in the linear regime (Kaiser 1987).

Non-linear corrections break the relation $\theta \equiv \nabla \cdot \mathbf{u} = \delta$, valid in linear PT. In particular, a similar calculation to that in Scoccimarro & Frieman (1996) for the density field shows that the critical index for the velocity divergence power spectrum is $n_c^\theta \approx -2$. Therefore, for the models under consideration with $n \approx -2$ one has $\theta = \nabla \cdot \mathbf{u} \sim \delta_L < \delta$; velocity fields are much more ‘‘linear’’ than the density field. We see from Eq. (11) that at small scales the J factors should suppress the regions undergoing turnaround, where $J \sim 0$. These regions, however, correspond to $1 = \nabla_z u_z \sim \theta/3 \sim \delta_L/3$, thus $\delta_L \sim 3$, which corresponds to very high values of δ and were suppressed already in real space by the exponential dependence on density. On the other hand, the effects of the pairwise velocity along the line of sight encoded in $e^{ik_z f \Delta u_z}$ plays a role, at high enough k_z oscillations of this factor damp power along the line of sight leading to a negative quadrupole to monopole

⁴In any case, even if there were higher-order corrections in ξ in Eq. (10), still what enters is the *non-linear* ξ , as shown in Scoccimarro (2001). Therefore, our arguments about the difficulties of determining the initial shape of the dark matter power spectrum from the forest still apply.

ratio, as in the case of the density field. However, since velocity fields should also display critical behavior as density fields, redshift space corrections should become very similar for models with different initial spectra. Therefore, we believe that the effects of velocities do not affect the conclusions above.

5. CONCLUSION

We have shown that at $z \sim 3$ the constraints on the primordial power spectrum of density perturbations that can be obtained from the Lyman alpha forest flux power spectrum are significantly affected by non-linear corrections to the evolution of the density perturbations. Because the primordial index of the power spectrum is so negative on the scales of interest non-linear corrections are much larger than naively expected. These corrections drive the power spectrum towards a critical slope, $n \approx -1.4$ irrespective of the primordial spectral index. This makes the determination of the primordial spectral index from measurements of the flux power spectrum particularly difficult.

If the objective is to constraint the slope of the primordial power spectrum, over a wide range of models in the relevant part of parameter space non-linear corrections are very large. Figure 4 shows that all the scales probed by the forest are significantly affected by the non-linear corrections for some shapes of the power spectrum. Thus, when trying to constrain cosmological parameters, the flux power spectrum cannot be used as a probe of the *linear* power spectrum of fluctuations at $z \sim 3$ except at the largest scales. Figure 1 illustrates how this “degeneracy” manifests itself when determining n_p , and figure 2 shows an example of two models with originally very different n_p that become almost indistinguishable due to non-linear evolution. This problem is made worse by the sensitivity of the bias to \bar{F} .

There are several ways to increase the sensitivity of the forest to the shape of the primordial power spectrum. First future improvements in measurements of the equation of state might help reduce the error on the shape. Second, the Sloan Digital Sky Survey (SDSS) has the capability of extending flux power spectrum measurements out to larger (and therefore more linear) scales, which will help towards tightening constraints on the shape of the power spectrum.

Acknowledgments: We thank Joop Schaye for useful comments and Enrique Gaztañaga for discussions about the behavior of C_{pq} in numerical simulations. We thank Patrick MacDonald for pointing out an error in the first manuscript. MZ is supported by David and Lucille Packard Foundation Fellowship for Science and Engineering and NSF grant AST-0098506. MZ and RS are supported by NSF grant PHY-0116590. LH is supported by an Outstanding Junior Investigator Award from the DOE and by NSF grant AST-0098437.

REFERENCES

- Bernardeau F. 1996, A&A, 312, 11
 Bernardeau F., Schaeffer, R. 1999, A&A, 349, 697
 Bi H. G., Davidsen A. F. 1997, ApJ, 479, 523
 Bryan G., Machacek M., Anninos P., Norman M. L. 1999, ApJ, 517, 13
 Cen R., Miralda-Escude J., Ostriker J. P., Rauch M. 1994, ApJ, 437, L9
 Choudhury, T. R., Srianand, R., Padmanabhan, T. 2001 ApJ, 559, 29
 Croft R. A. C., Weinberg D. H., Hernquist L., Katz N. 1997, ApJ, 488, 532
 Croft R. A. C., Weinberg D. H., Katz N., Hernquist L. 1998, ApJ, 495, 44
 Croft R. A. C., Weinberg D. H., Pettini M., Hernquist L., Katz N. 1999, ApJ, 520, 1
 Croft R. A. C., Weinberg D. H., Bolte M., Burles S., Hernquist L., Katz N., Kirkman D., Tytler D., 2000, astro-ph/0012324
 Frieman J. A., Gaztañaga E. 1999, ApJ, 521, L83
 Fry, J.N., Gaztañaga, E. 1993, ApJ, 413, 447
 Gaztañaga E. 1994, MNRAS, 268, 913
 Gaztanaga E., Croft R. A. C. 1999 MNRAS309, 885
 Gaztanaga E., Fosalba P., Croft R. A. C. 2001, astro-ph/0107523
 Gnedin N. Y., Hui L., 1996, ApJ, 472, 73
 Gnedin N. Y., Hui L., 1998, MNRAS, 296, 44
 Goroff M. H., Grinstein B., Rey S.-J., Wise M. B. 1986, ApJ, 311, 6
 Hernquist L., Katz N., Weinberg D. H., Miralda-Escude J. 1995, ApJ, 457, L5
 Hui L. 1999, ApJ, 516, 519
 Hui L., Gnedin N. Y. 1997a, MNRAS, 292, 27
 Hui L., Gnedin N. Y., Zhang Y. 1997b, ApJ, 486, 599
 Hui L., Rutledge R. E. 1999, ApJ, 517, 541
 Kaiser, N. 1987, MNRAS, 227, 1
 Kim T. S., Hu E. M., Cowie L. L., Songaila, A. 1997, AJ, 114, 1
 Lokas E.L., Juszkiewicz R., Bouchet F.R., Hivon E. 1996, ApJ, 467, 1
 Makino N., Sasaki M., Suto Y. 1992, Phys. Rev. D, 46, 585
 McDonald, P. & Miralda-Escude, J. 1999, ApJ, 518, 24.
 McDonald P., Miralda-Escude J., Rauch M., Sargent W. L. W., Barlow T. a., Cen R., Ostriker J. P., preprint astro-ph/9911196
 McDonald P., Miralda-Escude J., Rauch M., Sargent W. L. W., Barlow T. a., Cen R., Ostriker J. P., preprint astro-ph/0005553
 McDonald P., preprint astro-ph/0108064
 Machacek, M. and Bertschinger, E. 1995, American Astronomical Society Meeting, 186, 0207
 Meiksin A., White M. 2000, submitted to MNRAS, astro-ph 0008214
 Meiksin A., Bryan G., & Machacek M. 2001, astro-ph/0102367
 Miralda-Escude J., Cen R., Ostriker J. P., Rauch M. 1996, ApJ, 471, 582
 Miralda-Escude J., Haehnelt M., Rees M., 2000, ApJ, 530, 1
 Muecket J. P., Petitjean P., Kates R. E., Riediger R. 1996, A&A, 308, 17
 Narayanan V. K., Spergel D. N., Dave R., Ma C. P. 2000, ApJ, 543, L103
 Nusser A. 2000, MNRAS, 317, 902
 Nusser A., Haehnelt M. 2000, MNRAS, 313, 364
 Pichon, C., Vergely, J. L., Rollinde, E., Colombi, S., Petitjean, P. 2001, MNRAS, in press, astro-ph/0105196
 Rauch, M., Miralda-Escude, J., Sargent, W. L. W., Barlow, T. A., Weinberg, D. H., Hernquist, L., Katz, N., Cen, R. & Ostriker, J. P. 1997, ApJ, 489, 7
 Reisenegger A., Miralda-Escude J. 1995, ApJ, 449, 476
 Ricotti M., Gnedin N. Y., Shull M. 2000, ApJ, 534, 41
 Schaye J., Theuns T., Leonard A., Efstathiou G. 1999, MNRAS, 310, 57
 Schaye J., Theuns T., Rauch M., Efstathiou G., Sargent W. 2000, MNRAS, 318, 817
 Schaye J., astro-ph/0104272
 Scherrer, R. J., Weinberg, D. H. 1998, ApJ504, 607
 Scoccimarro R., Frieman J. A. 1996, ApJ, 473, 620
 Scoccimarro R., Couchman H.M.P., Frieman, J. A. 1999, ApJ, 517, 531
 Scoccimarro R. 2001, Acad. Sci. N.Y., 927, 13, astro-ph/0008277
 Theuns T., Leonard A., Efstathiou G., Pearce F. R., Thomas P. A. 1998, MNRAS, 301, 478
 Theuns T., Schaye J., Haehnelt M., MNRAS, 315, 600
 Theuns T., Zaroubi S., Tae-Sun Kim, Tzanavaris P., Carswell R., astro-ph/0110600
 Tegmark M., Zaldarriaga M., astro-ph/0002091
 Viel, M., Matarrese, S., Mo, H. J., Haehnelt, M. G., Theuns, T. 2001, MNRAS, in press, astro-ph/0105233
 Wadsley J. W., Bond J. R. 1996, Proceeding of the 12th Kingston Conference, eds. Clarke D., West M., PASP, astro-ph/9612148
 Wang X., Tegmark M., Zaldarriaga M., astro-ph/0105091
 White M., Croft R. A. C. 2000, ApJ, 539, 497
 Zhang Y., Anninos P., Norman M. L. 1995, ApJ, 453, L57
 Zaldarriaga M., Hui L., Tegmark M. 2001, ApJ, 557, 519
 Zaldarriaga M., Seljak U., & Hui L. 2001b, ApJ, 551, 48

